RESEARCH ARTICLE | JUNE 12 2023

The thickness effect on the compensation temperature of rare-earth garnet thin films

Special Collection: Ferrimagnetic Spintronics

Jing Ming Liang ; Xu Wen Zhao ; Yu Kuai Liu ; Pei Gen Li ; Sheung Mei Ng ; Hon Fai Wong ; Wang Fai Cheng ; Yan Zhou ; Ji Yan Dai ; Chee Leung Mak ; Chi Wah Leung

Appl. Phys. Lett. 122, 242401 (2023)
https://doi.org/10.1063/5.0150228

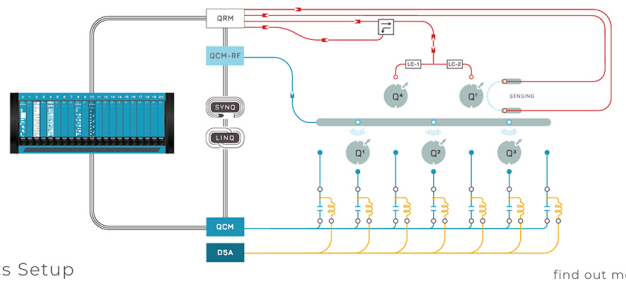

Applied Physics Letters ARTICLE pubs.aip.org/aip/apl

The thickness effect on the compensation temperature of rare-earth garnet thin films

Cite as: Appl. Phys. Lett. **122**, 242401 (2023); doi: 10.1063/5.0150228
Submitted: 13 March 2023 · Accepted: 1 May 2023 ·
Published Online: 12 June 2023

View Online Export Citation CrossMark

Jing Ming Liang,[1] Xu Wen Zhao,[1] Yu Kuai Liu,[2] Pei Gen Li,[1] Sheung Mei Ng,[1] Hon Fai Wong,[1] Wang Fai Cheng,[1] Yan Zhou,[3] Ji Yan Dai,[1] Chee Leung Mak,[1] and Chi Wah Leung[1,a)]

AFFILIATIONS

[1]Department of Applied Physics, The Hong Kong Polytechnic University, Hung Hom, Hong Kong, China
[2]College of Electronic Information and Mechatronic Engineering, Zhaoqing University, Zhaoqing 526061, Guangdong, China
[3]School of Science and Engineering, Chinese University of Hong Kong, Shenzhen, Guangdong 518172, China

Note: This paper is part of the APL Special Collection on Ferrimagnetic Spintronics.
[a)]**Author to whom correspondence should be addressed:** dennis.leung@polyu.edu.hk

ABSTRACT

The anomalous Hall effect measurements are used to probe the magnetization reversal of terbium iron garnet (TbIG) thin films at different temperatures. The compensation temperature (T_{comp}) of TbIG thin films is revealed, and the film thickness effect on the T_{comp} is studied. The results indicate a rise of T_{comp} along with decreasing film thickness. We postulate two possible origins for the observed behavior, namely interfacial element diffusion and strain effects between TbIG films and $Gd_3Ga_5O_{12}$ substrates. The results have implications for the study of spintronic devices based on ultrathin rare-earth iron garnet thin films.

There is intense interest in the spin Hall effect (SHE) based on ferrimagnetic oxide films.[1] Ferrimagnetic insulators (FMIs) are promising candidates for the new generation of memory device materials.[2] Under the action of SHE, when the FMI film is adjacent to a heavy metal (HM), charge flow in the HM layer can be converted into a spin current and transported into the FMI. Conversely, the spin current in the FMI can also be converted into a charge flow in the HM layer through the inverse spin Hall effect (ISHE).[3] The interaction between SHE and ISHE indirectly reflects the spin transport behavior in the magnetic film.

In addition to the SHE, the anomalous Hall effect (AHE) is another important phenomenon frequently studied in HM/FMI systems. It was reported that the magnetization reversal of FMI can be revealed through AHE measurement of the adjacent Pt layer, which is particularly useful when the magnetic properties are too weak to be detected with conventional magnetic measurement methods.[4,5]

Most research on HM/FMI is based on ferrimagnets with collinear magnetic sub-lattices such as yttrium iron garnet (YIG). In YIG, two Fe^{3+} from the octahedral sites and the tetrahedral sites are antiparallel with each other, with the tetrahedral-sites Fe^{3+} being dominant.[6] In some other iron garnets, rare-earth ions (RE^{3+}) substitute the Y^{3+} ions, and they tend to possess strong magnetic properties, particularly at low temperatures.[7] At certain temperatures, the magnetization of RE^{3+} (M_{RE}) and Fe^{3+} (M_{Fe}) cancel out due to their different temperature dependences,[8] and is termed as the compensation temperature (T_{comp}); experimentally, that is manifested as a temporarily vanishing magnetization. Some work[9,10] pointed out that the sub-lattice magnetization of REIG thin films demonstrates spin reorientation when the temperature is swept through T_{comp}.

Meanwhile, the thickness effect of REIG thin films on T_{comp} is rarely reported.[5,10,11] At the same time, the manipulation of T_{comp} is beneficial to the research and application of new-generation information storage devices, especially when T_{comp} can be achieved near room temperature.[12] As research pushes for thinner REIG films, the potential impact of film thickness on the measured T_{comp} should be clarified.

In this work, a systematic study was conducted to explore the thickness dependence on T_{comp} variation in Pt/TbIG bilayers by observing the AHE in the Pt layer. Our results have revealed a thickness dependence of T_{comp} in TbIG thin films. T_{comp} above room temperature is observed in TbIG films less than 7 nm. The possible origins of such a phenomenon are discussed.

TbIG films with thicknesses between 3 and 30 nm were deposited on (111)-orientated $Gd_3Ga_5O_{12}$ (GGG) single-crystal substrates by pulsed laser deposition. Subsequently, 5 nm Pt electrodes with a Hall bar pattern (channel width 160 μm, channel length 500 μm) were deposited by rf magnetron sputtering through a stainless-steel shadow

mask. The magnetic properties of the samples were measured by a vibrating sample magnetometer (VSM) module mounted on a physical property measurement system (PPMS, Quantum Design). The AHE resistances of the samples were also tested using the PPMS. Details concerning film deposition and characterization, device fabrication, and magnetic and transport measurement can be found in our previous work.[13]

The microstructure of TbIG films was probed by XRD, and the results of 2θ scans are shown in Fig. 1(a). Except for the 3 nm sample with no observable diffraction pattern due to the small film thickness, TbIG diffraction peak can be detected starting from a film thickness of 7 nm. The epitaxial nature of the samples is evidenced by other x-ray measurements (see Figs. S2–S4 in the supplementary material).

The 2θ values gradually shift to lower values with increasing film thickness, indicating a corresponding rise in the out-of-plane lattice constant (a_{out}) of TbIG.[14,15] The corresponding a_{out} values of the films are shown in Fig. 1(c). The Laue oscillations accompanying the TbIG peak also verify the high crystallinity of the thin films.[16] It is noted in Fig. 1(c) that a_{out} increases with increasing film thickness, which is contrary to expectation, as $a_{GGG} < a_{TbIG}$ and the strain would be relaxed as thickness increases. Meanwhile, the trend in Fig. 1(c) was also reported, and through a detailed scanning transmission electron microscopy (STEM) analysis, the effect was attributed to relaxations through localized interfacial distortions.[17,18]

The in-plane strain condition of a 30-nm sample was examined with asymmetric reciprocal space mapping (RSM) on the (642) lattice plane [Fig. 1(b)]. The reciprocal lattice plane of TbIG film is positioned directly below that of the GGG substrate with the same q_x value (0.2286 Å^{-1}), evidencing that the TbIG film is fully strained with an in-plane lattice constant ($a_{in} = \frac{2\sqrt{2}}{q_x}$) of 12.37 Å. Here, we define the in-plane and out-of-plane strains of TbIG films as $\varepsilon_{in} = \frac{a_{in}-a_0}{a_0}$ and $\varepsilon_{out} = \frac{a_{out}-a_0}{a_0}$, a_0 being the pseudo-cubic lattice constant of bulk TbIG in the garnet structure. Considering the films as fully strained, a_{in} of all samples should be consistent with that of GGG substrate and, hence, ε_{in} remains compressive and unchanged across samples. Meanwhile, ε_{out} [Fig. 1(c)] is tensile for all samples and rises gradually with increasing film thickness.

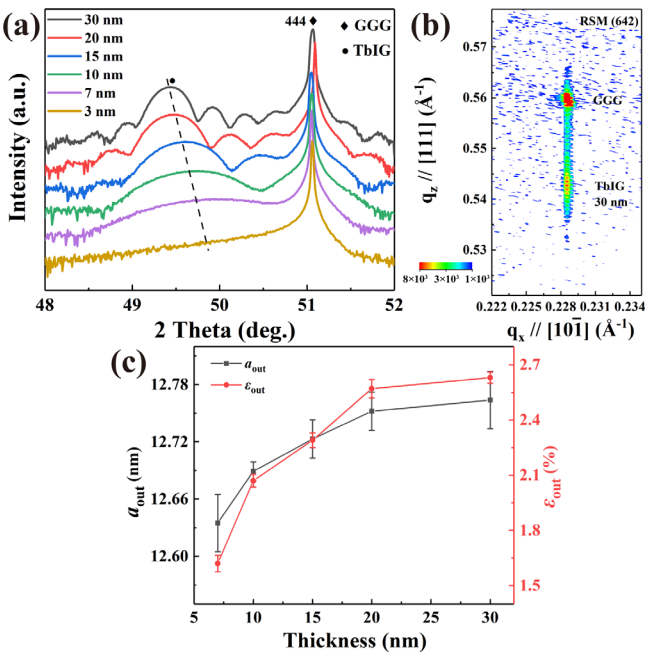

FIG. 1. (a) XRD 2θ scan of TbIG films with different thicknesses. (b) The RSM scan of (642) peak of TbIG (30 nm) on GGG (111). (c) a_{out} and ε_{out} values of TbIG films with different thickness.

Figure 2 shows the high-angle annular-dark-field (HAADF) scanning transmission electron microscopy (STEM) of TbIG (30 nm), as viewed along the [110] direction. The interface of the TbIG film and the GGG substrate can be identified in Fig. 2(a). The top surface of the film is very flat, which is consistent with atomic force microscope image of the sample (Fig. S1, supplementary material) that indicates a small surface roughness. No impurities or defects are found in the scanned area. The film thickness is confirmed to be around 30 nm. Figure 2(b) is an enlarged view of the selected area in (a), showing the TbIG layer is epitaxially grown on the GGG substrate.

Compositional mappings of the elements (Fe, Tb, O, Gd, and Ga) in the sample are presented by the energy-dispersive x-ray spectroscopy (EDX) in Fig. 2(c). Interlayer diffusions can be observed in Fe, Tb, Gd, and Ga, and a similar diffusion phenomenon has been reported in studies of YIG/GGG, in which Y and Gd can be regarded as the diffusion pair through the dodecahedral-site sublattice.[19–21] The element diffusion occurs across a region of around 4 nm (about 2 nm on each side of the interlayer), which agrees with previous reports.

The room temperature out-of-plane magnetic hysteresis loops (M-H loops) for TbIG films with thicknesses between 15 and 30 nm

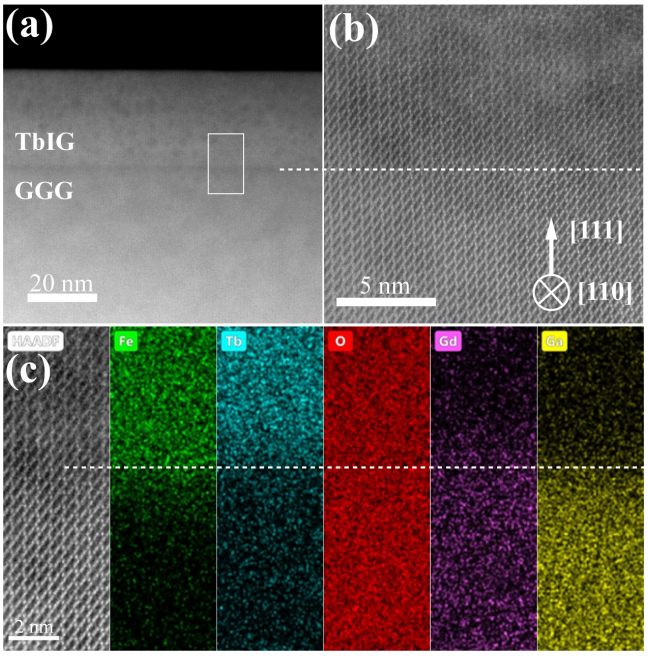

FIG. 2. (a) HAADF-STEM images of a TbIG (30 nm) thin film. (a) A cross-sectional STEM image, with high-magnification image of the selected region shown in (b). The white dashed line in (b) is a guide to the eye. (c) STEM-EDX mapping of Fe, Tb, O, Gd, and Ga.

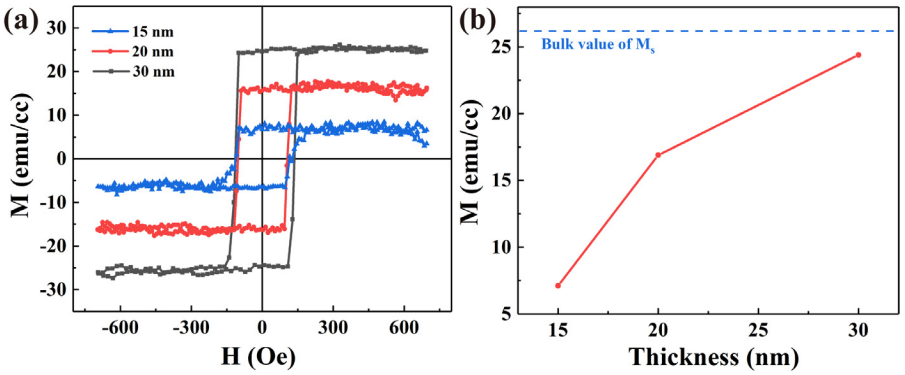

FIG. 3. (a) Out-of-plane M-H loops of TbIG films at room temperature. (b) M_s vs TbIG film thickness. Dashed line indicates the M_s value of bulk TbIG at room temperature.

are shown in Fig. 3(a). After subtracting the paramagnetic background from the GGG substrate, the M-H loops of all samples are square-shaped, indicating a strong perpendicular magnetic anisotropy.[22] For the 30 nm sample, the saturation magnetization (M_s) is about 24 emu/cc, which is slightly small than the bulk value (26 emu/cc).[23] The relationship between Ms and TbIG thickness is extracted and depicted in Fig. 3(b), and a reduction of M_s is observed when the film thickness is reduced. In particular, the M_s is only around 7 emu/cc for the 15 nm sample (which is 27% of the bulk value). Similar M_s reduction was also reported in the literature,[21] and various causes such as vacancies of Fe and O[24] and strain-induced perpendicular anisotropy[25] were postulated to cause such a behavior. The coercivity (H_c) of all three samples is about 100 Oe. The strong paramagnetic signal from the substrates prohibits the detection of signals from films thinner than 15 nm.

Figure 4(a) is the schematic of a 1/8 skeleton of TbIG unit cell, which shows the garnet structure of dodecahedral (*C*-site: Tb^{3+}), octahedral (*A*-site: Fe^{3+}), and tetrahedral (*D*-site: Fe^{3+}) sites. The temperature-dependent variations of sub-lattice magnetization in *C*-site Tb^{3+} (M_c), *A*-site, and *D*-site Fe^{3+} (M_a and M_d) are shown in Figs. 4(b)–4(d). At room temperature, M_a and M_d are antiferromagnetically coupled with a net magnetization direction along M_d, while M_c is ferromagnetically coupled with M_a.[26] Both the magnetizations of Tb and Fe ions decrease with increasing temperature, but the difference in their rate of decrease results in a competitive relationship. At temperatures far away from T_{comp}, the three sublattice magnetizations are collinear with M_d (M_c), taking the dominant contribution at $T > T_{comp}$ [Fig. 4(b)] ($T < T_{comp}$ [Fig. 4(d)]) range. At around T_{comp} [Fig. 4(c)], the three sub-lattice magnetizations develop a canted state.[10] Since the strength of M_c decreases more rapidly with increasing temperature, the three sublattice magnetizations compensate with each other and lead to a zero-saturation magnetization, accompanied by a vanishing AHE resistance.

The magnetization of TbIG films shows non-monotonic variation with temperature due to the existence of T_{comp}. This has impact on the spin-Hall AHE as measured in TbIG films in contact with heavy metals: in the measurement of the AHE resistance (R_{AHE}), the reversal of three sub-lattice magnetizations inside TbIG around T_{comp} is typically characterized by a sign change of the zero-field-R_{AHE} (R^0_{AHE}).[2,16,22,27]

Figure 5(a) shows the R_{AHE} vs field (R-H) loops of the Pt/TbIG (30 nm) sample between 10 and 300 K, with the (linear) ordinary Hall effect contribution being deducted. While squared R-H loops can be observed at most temperature points, at two temperatures the R_{AHE} signals are suppressed. One of them is around 210 K, which corresponds to the T_{comp} of TbIG.[23] The other R_{AHE} vanishing point (T_1) is around 145 K, which was similarly observed in other HM/FMI studies such as Pt/GdIG and W/TmIG.[11,27] The appearance of T_1 point was attributed to the competition of spin Hall effect-induced AHE and magnetic proximity effect-induced AHE, and is worth further investigations for verification.

The corresponding temperature dependences of R^0_{AHE} and H_c are extracted from Fig. 5(a) and plotted in Figs. 5(b) and 5(c). As shown in Fig. 5(b), the variation of R^0_{AHE} can be divided into three sections due to the presence of T_1 and T_{comp}. When $T > T_{comp}$ (300 ∼ 210 K), R^0_{AHE} monotonically decreases to zero with decreasing temperature. In between T_1 and T_{comp}, (210–145 K), R^0_{AHE} decreases to zero again with the decrease in temperature but with a sign change. Finally, for $T < T_1$

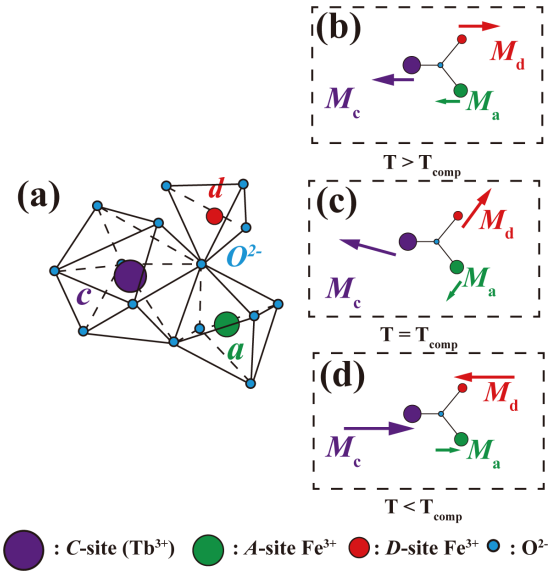

FIG. 4. (a) Skeleton diagram showing 1/8-unit cells of TbIG. The unit cell structure belongs to the garnet type with dodecahedral [*C*-site: Tb^{3+} (purple)], octahedral [*A*-site: Fe^{3+} (green)], and tetrahedral [*D*-site: Fe^{3+} (red)] sites. The oxygen sites (blue) are for reference only. (b)–(d) are schematics showing the sublattice magnetizations of *C*-site Tb^{3+} (M_c), *A*-site, and *D*-site Fe^{3+} (M_a and M_d) at different temperatures.

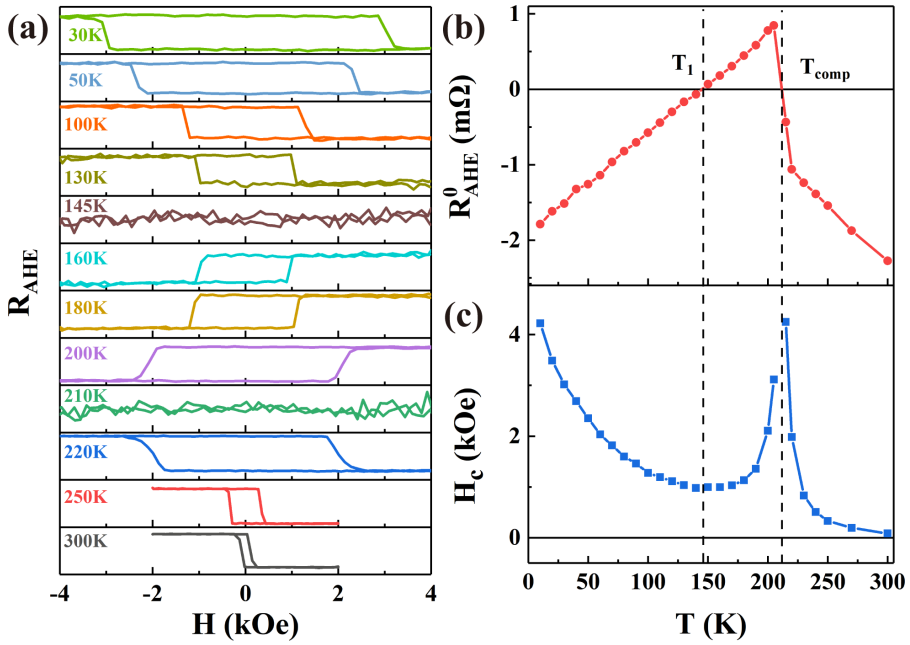

FIG. 5. (a) Selected R-H loops of the Pt/TbIG (30 nm) sample at different temperatures. The extract temperature dependences of R^0_{AHE} and H_c are shown in (b) and (c), respectively. Note that the y-axis scale of the R-H loops varies among the plots.

(145 ∼ 10 K), the R^0_{AHE} switches back to the same sign as at the 300 K and increases monotonically with decreasing temperature.

In addition, the temperature dependence of H_c [Fig. 5(c)] also shows a non-monotonic variation. The H_c drops with increasing temperature but demonstrates a strong divergence at 215 K, which further supports the occurrence of T_{comp}. A similar behavior has been reported in other studies.[16,28]

Central to the current study is the impact of TbIG film thickness on the AHE effect in Pt/TbIG system. The R^0_{AHE}-T and H_c-T curves of samples with varying TbIG thickness are summarized in Figs. 6(a) and 6(b), respectively. (Refer to the supplementary material for R-H loops for all samples at various temperatures.) For Pt/TbIG samples with a TbIG layer of thickness 10 nm or above, the R^0_{AHE}-T curves demonstrate sign crossover, one at 145 K for virtually all samples, and another one above 215 K. Based on the trend of the Pt/TbIG (30 nm) [Fig. 5(b)], we attribute the crossover at 145 K is the T_1 point, and the higher-temperature one being the T_{comp} of various samples. T_{comp} shows a clear rising trend with decreasing TbIG thickness. For Pt/TbIG (7 nm) sample, no obvious T_{comp} is observed up to our measurement limit of 340 K, as R^0_{AHE} indiscernible from the background was obtained starting at around 300 K; a dashed trendline is used in Fig. 6(a) for this part of the graph. For the Pt/TbIG (3 nm) sample, no distinguishable R_{AHE} signal can be observed at temperature beyond 200 K. It is possible that the TbIG magnetization becomes so weak in such samples that the R_{AHE} signal cannot be distinguished from the background signals at high temperatures.[21] We extract the T_{comp} of the four samples with thicknesses between 10 and 30 nm and plot the curves of the thickness dependence of T_{comp} in the inset of Fig. 6(a) for a clearer view.

The H_c-T plot in Fig. 6(b) for samples with 10–20 nm TbIG layer shows a similar trend with the Pt/TbIG (30 nm) sample. The H_c divergence for these samples confirms the T_{comp} increase with reducing TbIG thickness [Fig. 6(a)]. The apparently reducing peak H_c values with decreasing TbIG film thickness can be attributed to thickness

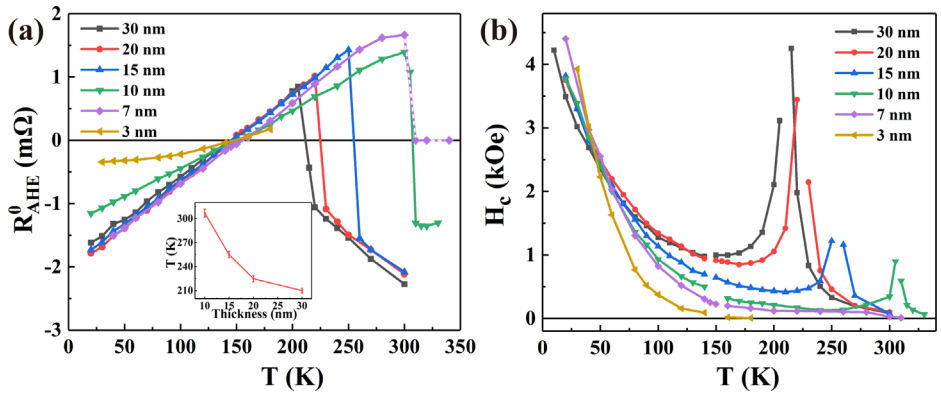

FIG. 6. The R^0_{AHE}-T (a) and H_c-T (b) curves of the TbIG films with different thickness. Inset of (a) shows T_{comp} of TbIG films with different thicknesses.

dependence of magnetocrystalline anisotropy commonly observed in magnetic films, although the mapping of the exact peak value proves impossible due to the vanishing R_{AHE} response at T_{comp}.

Here, we provide two possible origins for the observed T_{comp} variation with TbIG thickness, based on the lattice distortion and interfacial diffusion. Thickness dependent lattice distortion is commonly observed in thin films,[15,17,21,29] and the epitaxial strain varies based on the lattice mismatch between substrate and film materials.[30] TbIG films are subjected to in-plane compressive strain from the GGG substrate, which leads to out-of-plane tensile distortion. As the film thickness increases from 3 to 30 nm, the out-of-plane tensile strain increases gradually, which is manifested as the gradually increasing a_{out} in Fig. 1(c).

Theoretical model[12] points out that T_{comp} in REIG film can be tuned by film strain, and is attributed to the change of exchange coupling (J) between C-site RE^{3+} and D-site Fe^{3+} lattices (J values of other neighboring ion pairs are much smaller). When the lattice elongation increases, J decreases accordingly, and vice versa. The change of J is positively correlated with T_{comp}, i.e., the decrease (increase) of J leads to a corresponding drop (rise) of T_{comp}. This is consistent with the phenomenon observed in our samples, i.e., as the lattice distortion decreases, T_{comp} increases. The relationship between J and the strain of thin films was also reported in other studies. For example, first-principle calculations of YIG thin film pointed out that J of adjacent sub-lattices decreases with increasing sub-lattices spacing.[26]

The thickness dependence of T_{comp} can also arise from element diffusion between the GGG substrate and the TbIG film. Interfacial diffusion between garnet films and substrates was reported before,[19–21,31,32] with the interdiffusion range of several nm.[19,21] This results in an interfacial layer with gradient composition, potentially with different strain conditions as compared with the bulk of the film. Such gradient strain states have been observed in GdIG[32] and SmIG[33] deposited GGG substrates, which potentially change the exchange coupling between the C-site RE^{3+} and D-site Fe^{3+} ions. More importantly, the Gd element in the TbIG layer can contribute to additional magnetization signal, and this contribution becomes significant with decreasing TbIG layer thickness. Since T_{comp} of bulk GdIG (≈ 290 K)[34] is much higher than that of TbIG, T_{comp} of the film would be affected and shift to a higher temperature in case the Gd content increases in the film.

So far, REIG thin films have attracted a lot of attention in the study of spintronic, especially in some structures composed of ultrathin films.[35] However, as demonstrated in the current work, when the thickness is continuously reduced, the properties of the films change significantly.[36] Whether the material parameters are the same as those measured in thicker films is questionable. In particular, the variation of T_{comp} with film thickness was seldom mentioned. The prospect of tuning T_{comp} to near room temperature would benefit the studies and applications such as thermo-magnetic switching.[37] The current study highlights the need for careful analysis and characterization of ultrathin, and also demonstrates the T_{comp} of TbIG can be drastically different from the bulk.

In summary, epitaxial TbIG films with different thicknesses were deposited on (111)-orientated GGG substrates. The out-of-plane lattice constant increased with the film thickness due to the enhancement of the out-of-plane tensile strain. T_{comp} of the samples were revealed by AHE measurements, and a thickness dependence was demonstrated. Possible origins of such a thickness dependence were discussed. Our study is a timely reminder for the importance of careful characterization of ultrathin iron garnet films, which can be drastically different from the bulk behavior. On a positive side, careful manipulation of such variations would allow the exploration of enhanced T_{comp} of REIG thin films, which is beneficial for the research and application of spintronic devices.

See the supplementary material for microstructural characterization of TbIG/GGG and temperature-dependent R_{AHE} measurements of Pt/TbIG/GGG samples.

The authors acknowledge the financial support from the Hong Kong Polytechnic University (1-ZVWC, 1-CD6U), the Research Grants Council (Grant No: 15302320), the Research Fund of Zhaoqing University (No. 2021011832), and the Guangdong Special Support Project (No. 2019BT02X030).

AUTHOR DECLARATIONS

Conflict of Interest

The authors have no conflicts to disclose.

Author Contributions

Jing Ming Liang: Conceptualization (supporting); Data curation (lead); Formal analysis (lead); Investigation (lead); Methodology (lead); Writing – original draft (lead). **Chee Leung Mak:** Formal analysis (supporting); Funding acquisition (supporting); Resources (supporting); Supervision (supporting); Writing – review & editing (equal). **Chi Wah Leung:** Conceptualization (lead); Formal analysis (lead); Funding acquisition (lead); Project administration (lead); Resources (lead); Supervision (lead); Writing – review & editing (equal). **Xu Wen Zhao:** Investigation (supporting); Methodology (supporting); Writing – review & editing (equal). **Yu Kuai Liu:** Funding acquisition (supporting); Investigation (supporting); Methodology (supporting); Writing – review & editing (equal). **Pei Gen Li:** Investigation (supporting); Methodology (supporting). **S.M. Ng:** Investigation (supporting); Methodology (supporting); Writing – review & editing (supporting). **H. F. Wong:** Data curation (supporting); Investigation (supporting); Methodology (supporting). **Wang Fai Cheng:** Investigation (supporting); Methodology (supporting); Software (supporting). **Yan Zhou:** Formal analysis (supporting); Funding acquisition (equal); Resources (supporting); Writing – review & editing (equal). **Jiyan Dai:** Data curation (supporting); Methodology (supporting); Writing – review & editing (equal).

DATA AVAILABILITY

The data that support the findings of this study are available from the corresponding author upon reasonable request.

REFERENCES

[1]H. Nakayama, M. Althammer, Y. T. Chen, K. Uchida, Y. Kajiwara, D. Kikuchi, T. Ohtani, S. Geprags, M. Opel, S. Takahashi, R. Gross, G. E. Bauer, S. T. Goennenwein, and E. Saitoh, Phys. Rev. Lett. **110**(20), 206601 (2013); M. Althammer, S. Meyer, H. Nakayama, M. Schreier, S. Altmannshofer, M. Weiler, H. Huebl, S. Geprägs, M. Opel, R. Gross, D. Meier, C. Klewe, T.

Kuschel, J. M. Schmalhorst, G. Reiss, L. M. Shen, A. Gupta, Y. T. Chen, G. E. W. Bauer, E. Saitoh, and S. T. B. Goennenwein, Phys. Rev. B **87**(22), 224401 (2013).
[2]C. O. Avci, A. Quindeau, C. F. Pai, M. Mann, L. Caretta, A. S. Tang, M. C. Onbasli, C. A. Ross, and G. S. Beach, Nat. Mater. **16**(3), 309 (2017).
[3]Y.-T. Chen, S. Takahashi, H. Nakayama, M. Althammer, S. T. B. Goennenwein, E. Saitoh, and G. E. W. Bauer, Phys. Rev. B **87**(14), 144411 (2013).
[4]S. Meyer, R. Schlitz, S. Geprägs, M. Opel, H. Huebl, R. Gross, and S. T. B. Goennenwein, Appl. Phys. Lett. **106**(13), 132402 (2015); T. Shang, H. L. Yang, Q. F. Zhan, Z. H. Zuo, Y. L. Xie, L. P. Liu, S. L. Zhang, Y. Zhang, H. H. Li, B. M. Wang, Y. H. Wu, S. Zhang, and R.-W. Li, J. Appl. Phys. **120**(13), 133901 (2016).
[5]Y. Shiomi, T. Ohtani, S. Iguchi, T. Sasaki, Z. Qiu, H. Nakayama, K. Uchida, and E. Saitoh, Appl. Phys. Lett. **104**(24), 242406 (2014).
[6]T. Yamagishi, J. Awaka, Y. Kawashima, M. Uemura, S. Ebisu, S. Chikazawa, and S. Nagata, Philos. Mag. **85**(17), 1819 (2005).
[7]G. P. Espinosa, J. Chem. Phys. **37**(10), 2344 (1962).
[8]S. Geller, J. P. Remeika, R. C. Sherwood, H. J. Williams, and G. P. Espinosa, Phys. Rev. **137**(3A), A1034 (1965).
[9]M. U. Fayaz, M. S. Saleem, Y. Gu, X. Zhou, F. Pan, and C. Song, J. Appl. Phys. **126**(18), 183901 (2019).
[10]K. Ganzhorn, J. Barker, R. Schlitz, B. A. Piot, K. Ollefs, F. Guillou, F. Wilhelm, A. Rogalev, M. Opel, M. Althammer, S. Geprägs, H. Huebl, R. Gross, G. E. W. Bauer, and S. T. B. Goennenwein, Phys. Rev. B **94**(9), 094401 (2016); B. W. Dong, J. Cramer, K. Ganzhorn, H. Y. Yuan, E. J. Guo, S. T. B. Goennenwein, and M. Klaui, J. Phys. Condens. Matter **30**(3), 035802 (2018).
[11]S. Geprags, A. Kehlberger, F. D. Coletta, Z. Qiu, E. J. Guo, T. Schulz, C. Mix, S. Meyer, A. Kamra, M. Althammer, H. Huebl, G. Jakob, Y. Ohnuma, H. Adachi, J. Barker, S. Maekawa, G. E. W. Bauer, E. Saitoh, R. Gross, S. T. B. Goennenwein, and M. Klaui, Nat. Commun. **7**, 10452 (2016).
[12]T. Bayaraa, C. Xu, D. Campbell, and L. Bellaiche, Phys. Rev. B **100**(21), 214412 (2019).
[13]Y. K. Liu, J. M. Liang, H. F. Wong, S. M. Ng, C. L. Mak, and C. W. Leung, J. Magn. Magn. Mater. **536**, 168130 (2021).
[14]E. Lage, L. Beran, A. U. Quindeau, L. Ohnoutek, M. Kucera, R. Antos, S. R. Sani, G. F. Dionne, M. Veis, and C. A. Ross, APL Mater. **5**(3), 036104 (2017).
[15]B. Bhoi, B. Kim, Y. Kim, M.-K. Kim, J.-H. Lee, and S.-K. Kim, J. Appl. Phys. **123**(20), 203902 (2018).
[16]E. R. Rosenberg, L. Beran, C. O. Avci, C. Zeledon, B. Song, C. Gonzalez-Fuentes, J. Mendil, P. Gambardella, M. Veis, C. Garcia, G. S. D. Beach, and C. A. Ross, Phys. Rev. Mater. **2**(9), 094405 (2018).
[17]A. Krysztofik, S. Ozoglu, R. D. McMichael, and E. Coy, Sci. Rep. **11**(1), 14011 (2021).
[18]E. Popova, M. Deb, L. Bocher, A. Gloter, O. Stéphan, B. Warot-Fonrose, B. Berini, Y. Dumont, and N. Keller, J. Appl. Phys. **121**(11), 115304 (2017).
[19]A. Mitra, O. Cespedes, Q. Ramasse, M. Ali, S. Marmion, M. Ward, R. M. D. Brydson, C. J. Kinane, J. F. K. Cooper, S. Langridge, and B. J. Hickey, Sci. Rep. **7**(1), 11774 (2017).
[20]H. Chang, T. Liu, D. Reifsnyder Hickey, P. A. P. Janantha, K. A. Mkhoyan, and M. Wu, APL Mater. **5**(12), 126104 (2017).
[21]J. Mendil, M. Trassin, Q. Bu, J. Schaab, M. Baumgartner, C. Murer, P. T. Dao, J. Vijayakumar, D. Bracher, C. Bouillet, C. A. F. Vaz, M. Fiebig, and P. Gambardella, Phys. Rev. Mater. **3**(3), 034403 (2019).
[22]Y. K. Liu, H. F. Wong, K. K. Lam, K. H. Chan, C. L. Mak, and C. W. Leung, J. Magn. Magn. Mater. **468**, 235 (2018).
[23]E. Peter Wohlfarth, *Handbook of Magnetic Materials* (Elsevier, 1986).
[24]S. A. Manuilov, S. I. Khartsev, and A. M. Grishin, J. Appl. Phys. **106**(12), 123917 (2009).
[25]E. Popova, N. Keller, F. Gendron, M. Guyot, M. C. Brianso, Y. Dumond, and M. Tessier, J. Appl. Phys. **90**(3), 1422 (2001).
[26]L.-S. Xie, G.-X. Jin, L. He, G. E. W. Bauer, J. Barker, and K. Xia, Phys. Rev. B **95**(1), 014423 (2017).
[27]Q. Shao, A. Grutter, Y. Liu, G. Yu, C.-Y. Yang, D. A. Gilbert, E. Arenholz, P. Shafer, X. Che, C. Tang, M. Aldosary, A. Navabi, Q. Lin He, B. J. Kirby, J. Shi, and K. L. Wang, Phys. Rev. B **99**(10), 104401 (2019).
[28]M. Uemura, T. Yamagishi, S. Ebisu, S. Chikazawa, and S. Nagata, Philos. Mag. **88**(2), 209 (2008); C. D. Mee, IBM J. Res. Dev. **11**(4), 468 (1967).
[29]H. Wang, C. Du, P. Chris Hammel, and F. Yang, Phys. Rev. B **89**(13), 134404 (2014); M. Kubota, A. Tsukazaki, F. Kagawa, K. Shibuya, Y. Tokunaga, M. Kawasaki, and Y. Tokura, Appl. Phys. Express **5**(10), 103002 (2012).
[30]S. M. Zanjani and M. C. Onbaşlı, J. Magn. Magn. Mater. **499**, 166108 (2020).
[31]J. C. Gallagher, A. S. Yang, J. T. Brangham, B. D. Esser, S. P. White, M. R. Page, K.-Y. Meng, S. Yu, R. Adur, W. Ruane, S. R. Dunsiger, D. W. McComb, F. Yang, and P. C. Hammel, Appl. Phys. Lett. **109**(7), 072401 (2016).
[32]C. Holzmann, A. Ullrich, O.-T. Ciubotariu, and M. Albrecht, ACS Appl. Nano Mater. **5**(1), 1023 (2022).
[33]H. Yamahara, B. Feng, M. Seki, M. Adachi, M. Shamim Sarker, T. Takeda, M. Kobayashi, R. Ishikawa, Y. Ikuhara, Y. Cho, and H. Tabata, Commun. Mater. **2**(1), 95 (2021).
[34]P. Hansen, K. Witter, and W. Tolksdorf, Phys. Rev. B **27**(7), 4375 (1983).
[35]J. M. Gomez-Perez, S. Vélez, L. McKenzie-Sell, M. Amado, J. Herrero-Martín, J. López-López, S. Blanco-Canosa, L. E. Hueso, A. Chuvilin, J. W. A. Robinson, and F. Casanova, Phys. Rev. Appl. **10**(4), 044046 (2018); T. Nathan Nunley, S. Guo, L.-J. Chang, D. Lujan, J. Choe, S.-F. Lee, F. Yang, and X. Li, Phys. Rev. B **106**(1), 014415 (2022).
[36]C. A. F. Vaz, J. A. C. Bland, and G. Lauhoff, Rep. Prog. Phys. **71**(5), 056501 (2008).
[37]M. Deb, P. Molho, B. Barbara, and J.-Y. Bigot, Phys. Rev. B **97**(13), 134419 (2018); Y. Cao, S. Cao, W. Ren, Z. Feng, S. Yuan, B. Kang, B. Lu, and J. Zhang, Appl. Phys. Lett. **104**(23), 232405 (2014).